IEEE Access
Multidisciplinary | Rapid Review | Open Access Journal

Received April 22, 2022, accepted May 7, 2022, date of publication May 18, 2022, date of current version May 26, 2022.

Digital Object Identifier 10.1109/ACCESS.2022.3176450

Wave-Mode Configurable Ultrasonic Non-Destructive Evaluation System Using Optoacoustic Prism

MUHAMMAD AWAIS ABBASI AND HYOUNG WON BAAC, (Member, IEEE)
Department of Electrical and Computer Engineering, Sungkyunkwan University, Suwon 16419, Republic of Korea

Corresponding author: Hyoung Won Baac (hwbaac@skku.edu)

This work was supported in part by the Ministry of Science and ICT (MSIT), South Korea, through the Information Technology Research Center (ITRC) Support Program supervised by the Institute for Information & Communications Technology Planning & Evaluation (IITP) under Grant IITP-2022-2018-0-01798; and in part by the Basic Science Research Program through the National Research Foundation of Korea, funded by the Ministry of Education under Grant NRF-2020R1F1A1076828.

ABSTRACT We demonstrate a multi-mode ultrasonic non-destructive evaluation (NDE) system based on a hybrid transducer including an optoacoustic (OA) prism. In this system, the OA prism with a flexible curved transmitter is capable of not only generating acoustic signals with high OA conversion efficiency but also covering a wide angular range to initiate various acoustic wave modes into a specimen whose interface is in contact with the OA prism. The latter angular manipulation provides great flexibility for NDE, which is uniquely enabled by developing and employing the curved OA transmitter coated on the prism. Using finite-element-based simulation, we validate acoustic signal generation and propagation inside an aluminum specimen. Then, excitation, propagation, and acquisition of shear and Rayleigh wave modes are confirmed experimentally. As feasibility demonstration, our hybrid transducer system, consisting of the OA prism and a piezoelectric receiver, is utilized for NDE of an aluminum specimen which includes air void discontinuity of 5-mm diameter. This is realized by multi-mode acoustic excitation from the OA prism with incident angles of 33°, 42°, 47°, and 60°. This exhibits detection accuracy error less than 2% as confirmed by comparing calculated and measured time-of-flight values. Such OA prism-based realization of all range of angular wave modes allows our system to be potentially useful for NDE over broad metallic materials as long as their sound speed is faster than that of the OA prism, without causing additional reverberation noise commonly observed in conventional piezoelectric counterparts.

INDEX TERMS Optoacoustic prism, non-destructive evaluation, acoustic signal analysis, ultrasound transducer, shear wave, Rayleigh wave, flexible optoacoustic transmitter.

I. INTRODUCTION

Non-destructive evaluation (NDE) by utilizing a laser-generated ultrasound (LGU) technology has enticed an increasing attention over both academic and industrial fields. The technology has proven to be a three-dimensional (3D) NDE tool in various testing fields such as damage realization of carbon-fiber reinforced-plastic (CFRP) composites [1], weld discontinuities [2], pipelines monitoring [3], and evaluation of Li-metal batteries [4]. Ultrasound generation using continuous-wave (CW) laser beams, which are modulated, e.g., by mechanical choppers, has been extensively utilized for NDE [5]–[16]. In contrast to the CW-laser-based operation, pulsed laser sources with a few to tens of nanoseconds in temporal width have also been employed with an advantage of high-frequency bandwidth [17]. In order to realize a fully non-contact NDE system by using this LGU technology, several non-contact interferometers have been developed as detectors [18]–[20]. However, their inability for selective generation of a desired wave-mode necessitates the adoption of complex computational methods [21], [22]. Furthermore, due to low sensitivity, high laser intensity to sustain a signal-to-noise ratio (SNR) may cause thermal detriment to the target specimen [23], [24]. Instead of using the fully non-contact systems, an optoacoustic (OA) transmitter typically with a thin film form can be brought and attached onto

The associate editor coordinating the review of this manuscript and approving it for publication was Yingxiang Liu.

a specimen surface for its use as a source of ultrasound wave. Fiber-optic OA sources have been introduced for biomedical and NDE applications [25], [26]. However, these have suffered from limitations in OA conversion efficiency of transmitter film and only a single wave-mode generation due to a fixed fiber-tip arrangement. An all-optical system for rebar corrosion detection is developed by using gold nanoparticles layer as OA transmitter and fiber Bragg-gratings as sensors [27]. While the system effectively evaluated the steel rebar corrosion, this has constraints such as low laser damage threshold and conversion efficiency of metallic particles, complex design, and feasibility for only cross-sectional scanning. An OA system has been further developed for NDE applications, proposing a transducer impulse response probing method [28]. However, it can only be applied for thin cross-sectional scanning. It is also susceptible to thermal delamination of specimen due to direct laser beam irradiation. Although the above proposed systems have adopted OA-based configurations for NDE applications, they have a common drawback of fixed acoustic wave-mode generation: for example, one of longitudinal, shear and Rayleigh modes. Owing to the recent advancement in transmitter fabrication technology, nanocomposite-based OA transmitters with extraordinary OA conversion efficiency have been developed [29]–[36].

There are many types/modes of acoustic waves, *e.g.,* longitudinal waves, shear waves, Rayleigh waves, and Lamb waves. All these modes are very useful in NDE and have particular applications. The acoustic waves when interact with solid can travel as longitudinal waves or give rise to other wave modes, *e.g.,* shear, Rayleigh, and Lamb wave modes depending upon the incident angle and specimen thickness. However, for NDE applications, operation with a single acoustic wave-mode is preferred to eliminate diagnostic complication caused by multi-mode nature of acoustic waves. Therefore, this requires a capability of controlling an acoustic incidence angle in order to selectively launch a particular wave-mode, avoiding simultaneous existence of multiple modes. This angular manipulation can be realized by the inclusion of a wedge-shaped guide structure between acoustic transmitter and specimen. Snell's law allows the identification of the respective wave-mode:

$$\frac{\sin\theta_i}{\sin\theta_r} = \frac{v_w}{v_m} \tag{1}$$

where θ_i and θ_r are the incident angle in wedge and the refracted angle in test material, respectively. v_w is the speed of longitudinal wave in wedge, and v_m is the speed of respective wave-mode generated inside the test material. The speed of any wave-mode is unique for each material as a signature, depending on Young's modulus, Poisson's ratio, density, and temperature as well. Thus, a conventional triangular wedge allowing a single fixed operation angle can deviate from its respective mode-tuning capability in scenarios of temperature variation. A variable-angle wedge has been introduced for a piezoelectric ultrasound-based system, enabling to adjust an incidence angle and then a wave-mode [37]. However, its design required an additional movable block that should be attached at a transducer/wedge interface, inevitably increasing acoustic attenuation and causing extra wave-echo noise. An external wedge holder was also required to inhibit system disturbance [38]. Furthermore, due to design restriction, these systems cannot go beyond an incidence angle of 60° which can be required for realization of surface waves.

An LGU-based focused transmitter, fabricated by using a concave stainless steel mirror, has been reported for testing a 1-mm thick glass plate [39] by generation of Shear and Rayleigh wave-modes. An incident wave angle could be changed by rotating the focused transmitter. However, there were limitations in which the input laser beam was delivered only through a transparent side of the specimen. This is not desirable in most of the NDE applications. Moreover, water submergence of the whole system was also required in this configuration.

Similarly, miniature OA transmitter probes have been developed by using a dip-coating process to fabricate the end-face of a multi-mode fiber with gold-nanoparticle composite. These enabled non-destructive characterization of thin films [40] and corrosion quantification of reinforced steel bars [41]. However, these methods also have restrictions such as implementation of only a compressional wave-mode, water submergence, low optical absorption, and low laser damage threshold due to the use of metallic nanoparticles [33]. Recently, a partially non-contact system has been proposed by using candle-soot nanoparticle composite as an LGU transmitter together with a piezoelectric receiver [42]. However, a fixed angle wedge was adopted allowing only one wave-mode even for a fixed specimen material. Moreover, there were drawbacks such as the inhomogeneity in the candle soot deposition process and the limited availability in the choice of wedge material as it should endure the candle flame temperature of approximately 800-1400 °C.

In order to overcome the above limitations for OA transmitter-based NDE systems, we demonstrate an OA prism-based multi-mode ultrasonic NDE system using a nanocomposite-based flexible OA transmitter. The OA prism not only takes advantages of high OA conversion productivity and high damage threshold of the nanocomposite transmitter but more importantly allows excitation of all acoustic wave modes by providing a broad angular range of incidence. For the OA transmitter, a nanocomposite film based on a mixture of carbon nanotubes (CNTs) and polydimethylsiloxane (PDMS) was fabricated on a glass substrate and then transfer-coated conformably over a quarter cylinder wedge made of Rexolite used for multi-angle implementation. Shear and Rayleigh wave-modes were realized and comprehensively adopted for in-body and surface evaluations of a specimen (aluminum). Evaluation of these waves were performed by comparing simulated and experimental time-of-flight (ToF) values, which shows good agreement. Then, a defect scanning capability was demonstrated using a

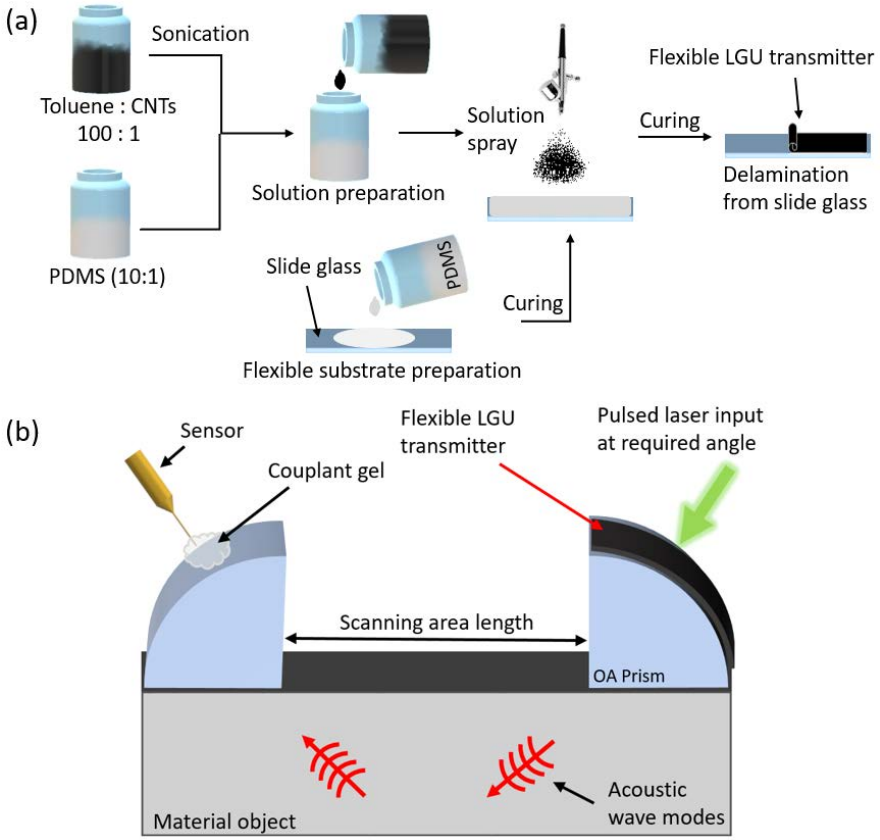

FIGURE 1. (a) Fabrication procedure of flexible CNTs-PDMS composite transmitter. (b) Configuration of the OA prism-based multi-mode NDE system. Dual quarter cylinder wedges are employed in each of transmitter and receiver side.

circular defect of 5-mm diameter located inside a specimen. Comparison of calculated and measured ToF values validated the proposed NDE system with an error less than 2%. All the experimental work was performed without water immersion. We expect that the OA prism-based hybrid transducer system can be applied to a broad range of test materials, as long as their sound speed is faster than that of the prism, owing to its angular controllability without causing any disturbance and additive acoustic attenuation.

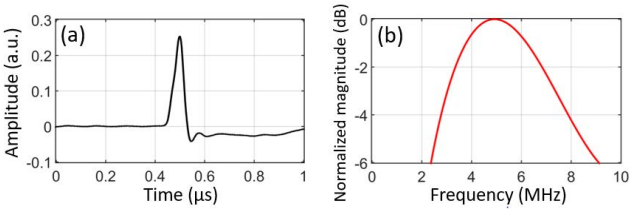

FIGURE 2. (a) The forward waveform profile detected in a near-field incidence condition to the detector. (b) The frequency spectrum obtained from (a) showing a center frequency of 5 MHz and a 6-dB bandwidth of ~6.5 MHz.

II. MATERIALS AND METHODS

A flexible OA transmitter was fabricated by using CNTs as optical absorbers and PDMS as an elastomer matrix for thermal expansion. PDMS has been comprehensively employed in OA transmitters due to its extraordinary volumetric coefficient of thermal expansion (9.2×10^{-4} K^{-1}) [33]–[36], [40]–[42]. Furthermore, the CNTs-PDMS nanocomposite combination has also been reported for high OA conversion efficiency as compared to other carbon nanoparticles [35]. For fabrication process of the transmitter, a solution-spray method was employed (Figure 1(a)). Initially, a transparent and flexible substrate (~0.5-mm thickness) was fabricated on a glass slide with dissolved and degassed PDMS (Sylgard 184 from Dow Corning, polymer: curing agent~10:1 wt%) by using a drop-casting method. A mixture of multi-walled CNTs (length: 1.5~2 μm, diameter: 15~20 nm) and toluene (toluene: CNTs; 100:1 weight ratio) was also prepared and then sonicated for 2 hours for homogeneous dissolution of CNTs. Then, the PDMS obtained in similar composition (10:1) was blended with a toluene-CNTs mixture in a 1:1 ratio of weight, to form a nanocomposite solution. This solution was sprayed onto the PDMS substrate prepared earlier. The toluene was rapidly evaporated at room temperature, while the sprayed CNTs with PDMS were concentrated on the cured substrate surface. Finally, after curing the sprayed solution at 90 °C for 15 minutes, the substrate was delaminated from the glass slide to obtain the flexible transmitter.

An overall configuration of the OA prism-based multi-mode NDE system is shown in Figure 1(b). A selected spot by pulsed laser irradiation (indicated by the green arrow) determines a source position of acoustic wave on the curved OA transmitter which is transfer-coated on the quarter cylinder wedge. The acoustic wave is then delivered through the right wedge/specimen, leading to a specific propagation mode within the specimen.

CNT-PDMS transmitters with glass substrates have been analyzed previously [31], [33]. We characterized our flexible transmitter without prism (*i.e.,* water/CNT-PDMS/PDMS/air) by measuring a time-domain OA waveform and analyzing its frequency spectrum in a near-field incidence condition to the detector. The gap between transmitter and detector was <1 mm, with a laser beam size of 5-mm diameter and a laser energy of 8 mJ/pulse. Upon laser excitation, the OA transmitter generated two wavefronts propagating forward and backward. The backward wave propagates across the CNT-PDMS film and then reflects back from air, then following the forward wave with a round-trip time delay [43]. Due to a temporal gap between both waves (measured as 1.25 μs), we selected the forward wave only in our characterization. Figure 2(a) and 2(b) show the detected forward waveform upon laser irradiation and its frequency spectrum, respectively, with a center frequency of 5 MHz and a 6-dB bandwidth of ∼6.5 MHz.

The simplest approach to boost the output acoustic pressure from an OA transmitter is by increasing the input laser fluence [35]. However, the maximum possible input fluence is limited by the laser induced damage threshold of the transmitter material. Thus, the maximum-output pressure can be determined with the laser fluence at the damage threshold. Our fabrication approach allowed a significantly high threshold value of 174∼214 mJ.cm^{-2}. The damage threshold was characterized by using a setup and procedure reported previously [36].

For preparation of the OA prism substrate, a quarter cylinder wedge was fabricated by using the Rexolite (cross-linked polystyrene) which is lightweight, chemically resistant, and corrosion resistant. It also has negligible outgassing, a low sound speed, and an extremely low attenuation even for high frequencies (e.g., 1.1dB/mm at 30 MHz) [44]. Due to these distinctive properties, it is suitable for a broader range of acoustic frequencies and environmental conditions. This also enables to initiate various acoustic wave-modes in metals typically having high sound speeds: for example, aluminum, steel, brass, and copper. We adopted two symmetric intermediate wedges on both transmitter and receiver sides. Furthermore, the acoustic impedance of Rexolite (∼2.5 MRayls) is in a compatible range for the PDMS-based nanocomposite (∼1.5 MRayls), ensuring a low reflection loss at the transmitter-wedge interface (25%).

A schematic interpretation of the implemented experimental setup is shown in Figure 3. A Q-switched Nd: YAG laser beam (Litron Laser, UK) was used with 532-nm wavelength, 7-ns pulse width, 10-Hz repetition rate and 8-mm beam diameter. An aluminum specimen portion (50-mm length, 40-mm width, and 25-mm height) was evaluated by using our system. Dual quarter cylinder wedges as acoustic prisms (50 mm in a cylindrical radius) were symmetrically placed with a 50-mm scanning length between them. A very thin layer of acoustic couplant gel was coated between each wedge and specimen. The flexible OA transmitter was made in contact with the input prism using the couplant gel, covering an angle range up to 90°. Two mirror reflectors were adjusted to propagate the laser beam in the direction of transmitter. The mirror was rotated to control the incident laser beam angle towards the curved transmitter. On the receiving side, a needle-type hydrophone of polyvinylidene fluoride (PVDF) was placed with an end-face diameter of 1 mm (NH1000, Precision Acoustics, UK) along with its pre-amplifier (3-dB bandwidth: 10 kHz to 50 MHz) and a DC coupler. The hydrophone position was controlled by using a 3-D arm and adjustable rotating clamp to make a required angle of detection along the curvature. Instead of making a direct contact with the prism, the detector end was maintained with a gap of approximately 3 mm from the curved surface of wedge, which was covered by the couplant. To monitor and record an output signal, the PVDF hydrophone was connected to a digital oscilloscope (LeCroy WaveSurfer 452, Chestnut Ridge, USA) through a pre-amplifier. Detected time-domain waveforms were then recorded by taking an average of 50 signal traces.

TABLE 1. Material properties used in the simulation model.

Property / Material	Density (Kg/m^3)	Young's modulus (GPa)	Poisson's ratio	Sound speed (S_L)[a] (m/s)
Rexolite	1050	2.3	0.42	2337
Aluminum	2700	70	0.33	6180

[a]S_L = Longitudinal sound speed (measured)

In order to realize the system application for non-destructive detection of a defect through incident angle variation, we used a specimen containing an air void defect (a cylindrical hole with 5-mm diameter). The defect was situated at the center of the gap between two prisms (60 mm) and in the depth of 15 mm.

III. RESULTS AND DISCUSSION

The proposed system was validated through a time-domain simulation model analysis, conducted by using a finite element method (FEM) (COMSOL Multiphysics, Version 5.6, Burlington, USA). A two-dimensional (2-D) simulation model was built to test an aluminum specimen by using acoustic prisms in contact to the specimen surface (Figure 4). The simulation was performed to visualize angular generation of acoustic waves, wave-mode initialization in specimen, and wave propagation throughout the whole system. A free-triangular mesh type was applied with a maximum element size of ∼0.1 mm. All the dimensions for specimen and

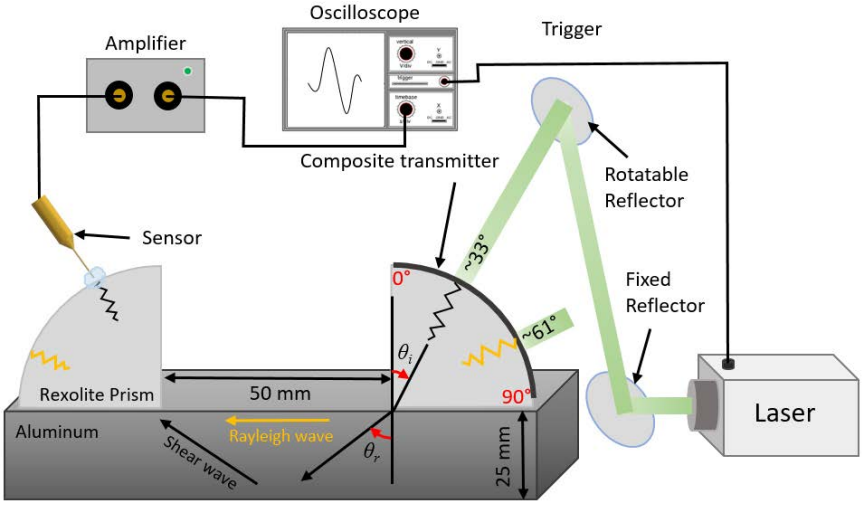

FIGURE 3. A schematic interpretation of experimental setup for ultrasonic characterization of the system. Incident and refracted angles, in the input prism and specimen, are denoted as θ_i and θ_r respectively.

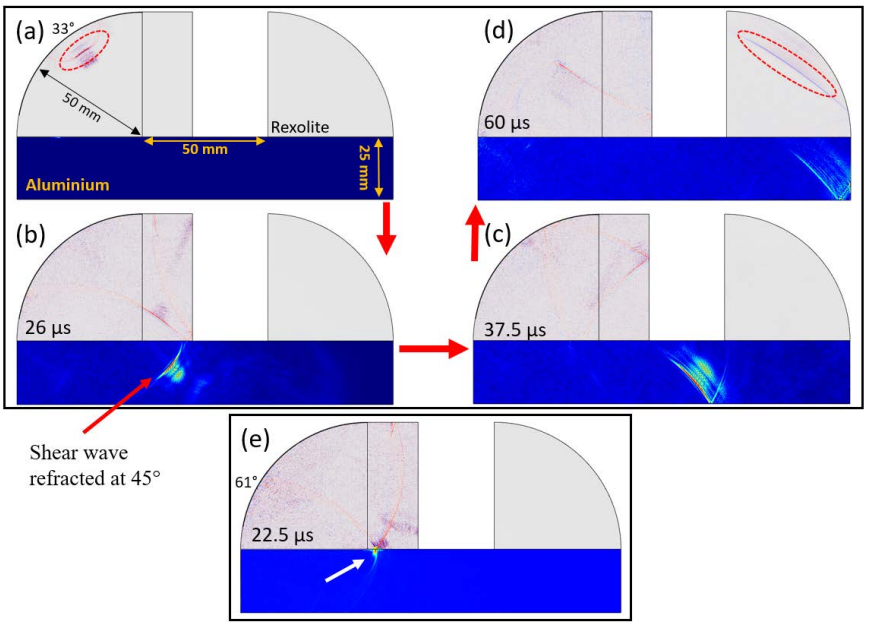

FIGURE 4. Visualization for spatio-temporal transition of acoustic wave-modes initiated from multiple incident angles (calculation). Note that the input prism is on the left side and the output prism on the right side. The instantaneous moment of wave is shown with each ToF value written at the left bottom of each figure. (a-d) Propagation of shear wave-mode spawned inside the test sample with incident and refraction angles of 33° and 45 ° (red arrow), respectively. (e) Emergence of the Rayleigh wave (indicated by white arrow) at ToF = 22.5 μs obtained by using an incident angle of 61° which is greater than the second critical angle (50°) between prism and specimen.

prism were set to agree with values used in the experimental configuration. The material properties used in the simulation model are shown in Table 1. The curved transmitter surface of the left prism (here, placed at the left side) was divided into multiple spatial segments (each segment length: ~5 mm) covering from 0° to 90°. To apply a certain required angle of incidence from the input prism surface, a single segment at the defined angle was selected as an acoustic source. The COMSOL modules of pressure-acoustics and solid-mechanics were used for acoustic wave generation and propagation in the solid aluminum specimen, respectively. We applied an elastic force equation to the corresponding curved surface segment of the prism for generation of acoustic wave. An acoustic pressure wave p(t) from the source was initiated by using the following expressions [35],

$$Q_{as} = \left[\nabla^2 - \frac{1}{c^2}\frac{\partial}{\partial t^2}\right] p\,(t) \tag{2}$$

$$p\,(t) = g\,(t)\,e^{i2\pi f_c t} \tag{3}$$

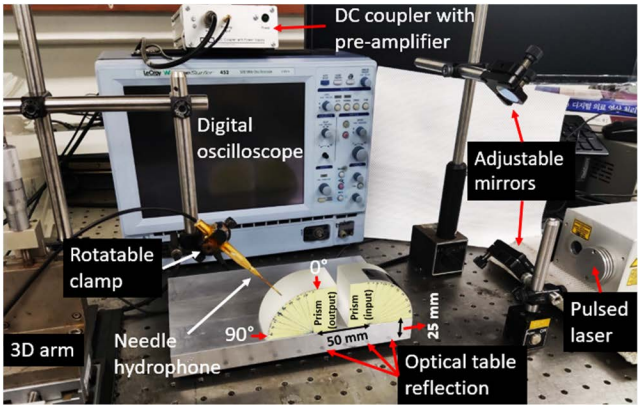

FIGURE 5. OA prism-based multi-mode ultrasonic NDE system using dual quarter cylinder wedges. The prisms are marked for respective angles of curved surface (0° to 90°). Any required incident angle can be defined and excited by the input laser beam irradiation onto a specific spot of OA transmitter attached to the input prism (right-upper side). The couplant gel covers a gap of 3 mm between output prism (left-upper side) surface and hydrophone sensor. This setup shows the identical arrangement with that of the simulated model (Figure 4).

where Q_{as} and c are the elastic force to generate acoustic waves and the speed of sound, respectively. Here, g(t) is the temporal Gaussian distribution function with a full-wave-at-half-maximum (FWHM) width of ∼7 ns to match the laser beam pulse profile, and f_c is the center frequency of the source selected as 5 MHz.

The 1st and 2nd critical angles (θ_{cr1st} and θ_{cr2nd}) at the prism/specimen interface were calculated by using Snell's law: ∼22° and ∼50°, respectively. Our simulation demonstrates spatio-temporal wave propagation throughout the structure as shown in Figure 4. The incident angles of 33° ($> \theta_{cr1st}$) and 61° ($> \theta_{cr2nd}$) were employed to initiate shear and Rayleigh wave-modes, each of which allows evaluation within the specimen (in-body scan) and at the surface. Figure 4(a-d) show each stage of wave propagation: longitudinal wave emergence in the left-side prism (at 33°), its conversion to shear wave-mode at the prism /specimen interface, reflection from the other edge, and again refraction into the right-side prism to be detected at the same angle on the surface, respectively. The red circles in the prisms indicate the acoustic wavefronts. The obtained total ToF was 65.60 μs at the right (output) prism surface. Propagation of the Rayleigh wave-mode was also realized along the surface, which is initiated at an incident angle of 61° in the same model. Figure 4(e) presents the Rayleigh wave appearance on the specimen surface at 22.5 μs (white arrow). The Rayleigh wave was detected at the ToF of 60.3 μs. Thus, the design parameters of the suggested NDE system were well validated through our simulation. Moreover, this ensures that multiple wave-modes can be controllably initiated using the OA-prism configuration.

Next, the proposed multi-angle NDE system was experimentally verified by using the same design parameters as in the simulation model. A real image of the system configuration is shown in Figure 5. The input (right) and output (left) arrangement of prisms is opposite here to that of Figure 4. A laser pulse with the Gaussian profile was used to excite the OA transmitter with a diameter of 5 mm and a pulse energy of 8 mJ throughout the experiment. A rotatable reflection mirror was adjusted to set an input laser beam angle above the curved flexible transmitter: 33° for the shear wave-mode and then 61° for the Rayleigh wave-mode implementation.

Comparison of simulated and experimental results for the executed wave-modes is presented in Figure 6. The first shear and Rayleigh wavefronts were found at ToF = 67.85 μs (Figure 6(a)) and 62.55 μs (Figure 6(c)), respectively, followed by the succeeding reverberation noise. Commonly for both wave-modes, a time delay of approximately ∼2.3 μs was found for the measured wavefronts. This is because the simulation does not take into account the gaps by the external couplant gel placed at two interfaces of transmitter/prism and detector/prism. Except these gaps, the first arriving wavefronts are found in a good agreement with the simulated results in terms of waveform profiles and ToF values. The forward/backward wave generation effect, as explained in the previous section, can be seen in Figure 6(a) (indicated by the red arrows) of experimental results in form of a wavefront pair generated by a single laser pulse.

Finally, we utilized the proposed system for NDE of an aluminum specimen containing a circular hole (defect) of 5-mm diameter. The specimen was completely tested through in-body and surface scans by varying incident acoustic wave angles with optical beam manipulation. Incident angles (θ_i) of 33° and 47° were implemented step by step to emerge shear wave for in-body evaluation of specimen, leading to refraction angles (θ_r) of 45° and 67°, respectively. For surface evaluation, Rayleigh wave was also introduced. Figure 7 fully demonstrates how the defect detection is performed by presenting initiated wave-modes for respective angles (differentiated by colors), their propagation paths, covered distances in specimen, and measured output waveforms. The total ToF (T_{total}) for each wave-mode was estimated by using the following expression:

$$T_{total} = \sum T_i = 2T_P + T_s + T_g$$
$$T_i = \frac{d_i}{v_i} \quad \text{where } i = p, s, \text{ or } g. \tag{4}$$

For the i-th medium, T_i, d_i, and v_i denote ToF, the propagated distance, and the wave velocity. Also, T_p, T_s, and T_g are ToF in prism, ToF in specimen, and ToF in couplant gel, respectively. The shear and Rayleigh wave velocities in the specimen are 3020 and 2718 m/s, respectively. In case of Rexolite prism, the longitudinal wave velocity was measured as 2337 m/s.

The estimated propagation paths and distances covered in the specimen by the initiated shear waves are shown in Figure 7(a). For instance, in case of laser beam irradiation at the angle 33°, a shear wave was estimated to travel a distance of 42.42 mm up to the other edge of the specimen with the refraction angle of 45°. Thus, after reflection from the

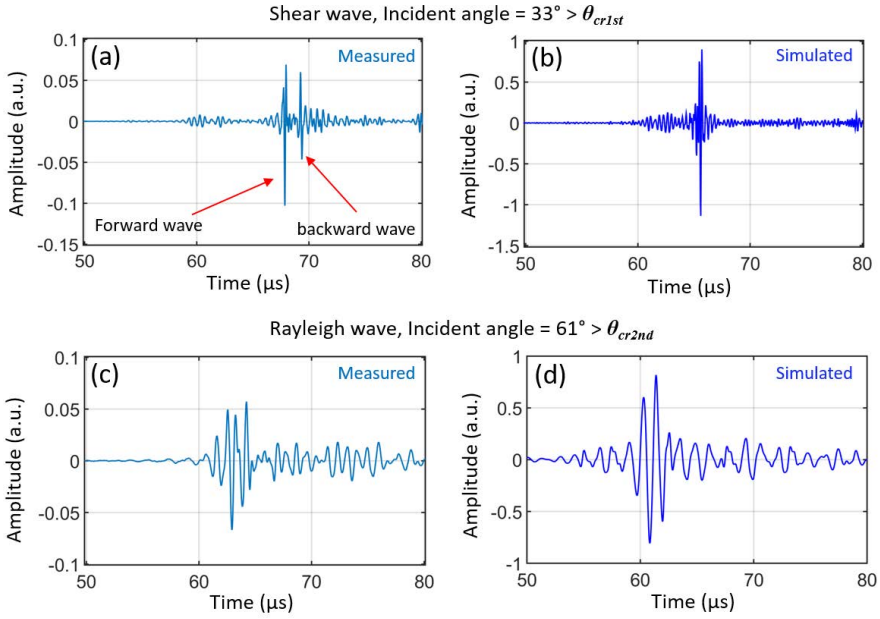

FIGURE 6. Comparison of simulation and experimental results. (a) and (b): Measured and simulated shear-mode waveforms, respectively (ToF = 67.85 and 65.6 μs for the first-arrived wavefronts); (c) and (d): Measured and simulated Rayleigh waveforms (ToF = 62.55 and 60.3 μs). A time delay of ~2.3 μs between measured and simulated peak positions is commonly observed for both shear and Rayleigh wave-modes, which is due to the gaps by the external couplant gel at the transmitter/prism and detector/prism interfaces (the gaps included in the measurement only).

TABLE 2. Comparison of calculated and measured ToF values.

Incident angle	Refracted angle	Wave mode	Travel distance in specimen (mm)	Wave speed (m/s)	*Total ToF (μs)	
					Calculated	Measured
33°> θ_{cr1st}	45°	Shear	84.84	3020	73.54	72.30
47°> θ_{cr1st}	67°	Shear	65.00	3020	66.96	65.90
60°> θ_{cr2nd}	90°	Rayleigh	60.00	2718	67.51	66.50

*Total ToF = $2T_P + T_s + T_g$

specimen/air boundary at the other edge, the total distance of 84.84 mm inside the specimen was obtained before reaching at the output prism interface. From the distance estimation inside the prism and the couplant gel, the total ToF for 33° was calculated as 73.54 μs. In the similar manner, a shear wave generated at 47° angle was reflected from the circular defect, covering a distance of 65 mm inside the specimen with a total calculated ToF of 66.96 μs up to the detector position. The Rayleigh wave was estimated to cover a distance of 60 mm along the specimen surface with a calculated total ToF of 67.51 μs. The experiment was executed after making all these pre-calculations. Figure 7(b-d) depict the measured waveforms with their respective ToF for the first-arrived wavefront.

Lastly, the intermediate incident angle of 42° was also implemented to check partial wavefront deflections from the defect and the other edge of specimen. The received waveforms by the detector are presented in Figure 7(e). Two pulsed waveforms were detected with ToF = 65.9 and 72.4 μs, respectively. Each pulse was obtained by partial reflection from the defect and the opposite edge. This is confirmed by the ToF values of acoustic waves separately measured in Figure 7(b) and 7(c). Table 2 compares the calculated and measured ToF together with other estimated parameters. The measured total ToF values were within a difference of 2% with the calculated values.

For a comparative analysis between our angular OA prism-based system and a conventional fixed-angle wedge, we also performed simulation using conventional fixed-angle wedges with size dimensions similar to those used for our proposed prism (i.e., height = width = 50 mm). Here, instead of a curved surface for the prism, we provided a flat surface at a fixed angle of ~33°, which is typically available in conventional systems. The fixed-wedge simulation results (Figure 8) shows that the ToF result with the fixed-angle wedges (66 μs) almost agrees with that of the proposed system using OA prisms (65.6 μs; in Figure 6(b)). These comparative simulation results confirm the validity of our proposed prism for wave-mode configurable operation over a wide angular range.

The proposed OA prism-based multi-mode NDE system is capable to initiate all ultrasound wave modes by varying

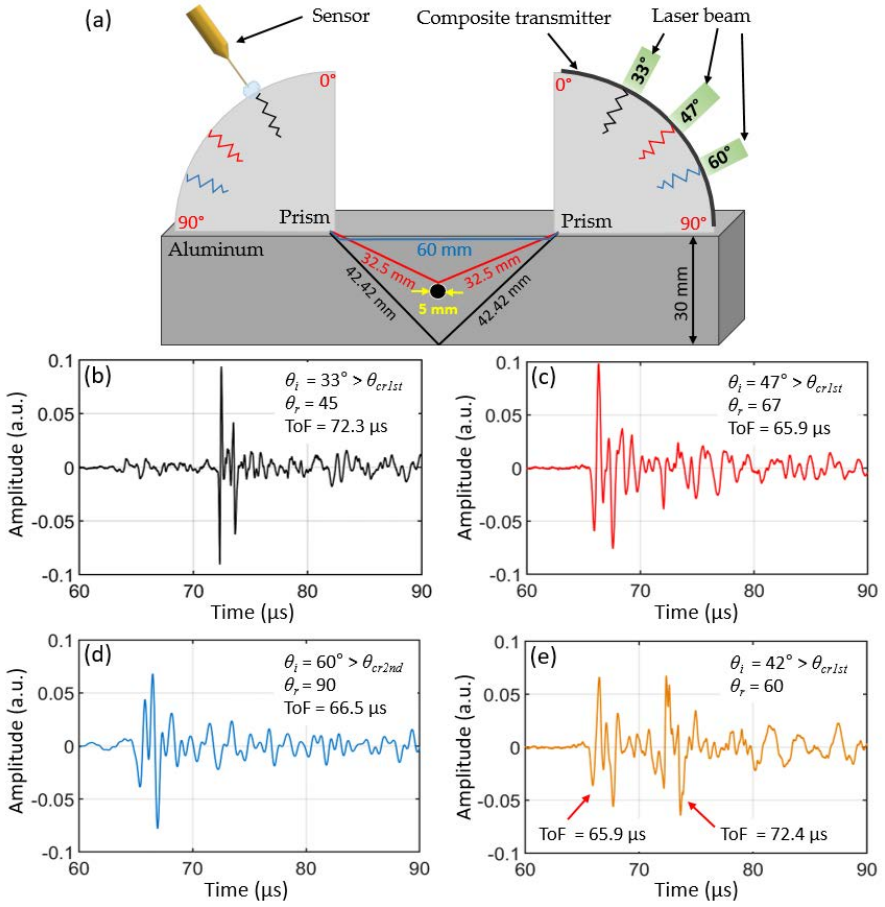

FIGURE 7. A full pictorial demonstration of the NDE application by non-contact multi-angle realization through laser-beam manipulation. θ_i is the incident angle in prism (33°, 47°, 60°, and 42°), and θ_r the refracted angle in specimen (45°, 67°, 90°, and 60°), respectively. (a) A schematic view of the system execution. This has a gap of 60 mm between both prisms. Each wave for the respective incident angle is indicated by different colors (shear wave - black and red; Rayleigh wave - blue). For each wave, the estimated propagation path, the propagated distance inside the specimen, and the point of reflection are also shown. (b-d) Graphical representation of measured waveform profiles. The relevant θ_i, θ_r, and the measured ToF of the first wavefront are also denoted. (e) The output waveform for the incident angle of 42° is shown. Two pulsed waveforms are resulted from partial reflections from the defect and the opposite edge of prism. Their corresponding ToF values (indicated by red arrows) agree with those of waves separately detected from the similar reflection points in (b) and (c).

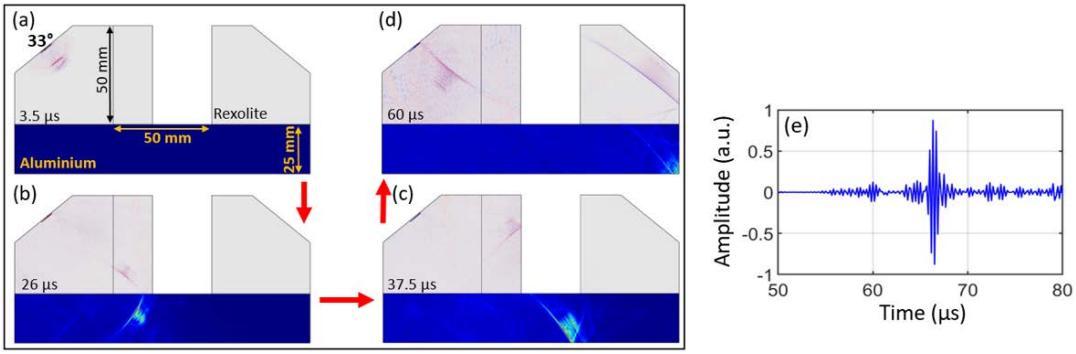

FIGURE 8. Realization of a fixed-angle wedge execution at an angle of 33° (simulation; the input wedge located on the left side and the output wedge on the right side). The instantaneous moment of shear wave is shown with each ToF value written at the left bottom of each figure. (a-d) Propagation of shear wave-mode emerged inside the test sample with a fixed incident angle of 33°. (e) The obtained signal at the output wedge surface (right side) (ToF = 66 μs).

the incident wave angle. This is achieved by adopting a curved surface prism with a flexible OA transmitter, and then controlled by the input laser-beam manipulation. It is difficult to realize such non-contact and wide range angular

adjustment without causing any system disruption and additional reverberation by using conventional piezoelectric-based variable wedges [37], [38]. In case of LGU, the previously reported rotatable metal-based focused OA transmitter required a very high laser energy (180 mJ/pulse) due to its low thermal coefficient of expansion. This was available only with transparent test samples to conduct laser-beam irradiation towards a transmitter front face [39]. Miniature OA transmitters, fabricated by using gold-nanoparticle composites, have also been demonstrated for non-destructive characterization [40] and corrosion quantification [41]. However, these systems have limitations of fixed wave-mode generation, low optical absorption, and low laser damage threshold due to the use of metallic nanoparticles. Comparatively, our proposed flexible nanocomposite transmitter possesses high OA conversion efficiency together with a high laser damage threshold of 214 $mJ.cm^{-2}$. The high OA efficiency of the system enables the input laser energy of only 8 mJ/pulse to excite sufficiently strong transmitted acoustic signal to be detected by the sensor without making a direct contact with the prism surface. This ability makes the sensor less vulnerable to damage in industrial environments which are exposed to random physical vibrations and electric leakage from a specimen. Moreover, our system does not require water immersion of the whole setup used in the conventional systems. Recently, an LGU-based system with candle-soot nanoparticles composite transmitter has also been developed for partially non-contact testing [42]. However, it has the constraints of fixed angle (43°) wedge with material limitations to tolerate high temperature of candle flame for nanoparticle deposition.

The structural stability of the detection configuration is required to ensure the measurement repeatability. The current detection system utilizes the 3-D arm for spatial adjustment and a rotatable clamp for angular control of hydrophone position. We confirmed the consistent ToF values through multiple measurement scans on the curved surface. For example, in Figure 6(c), the average ToF value of the Rayleigh wave for 5 repeated measurements was 62.55 μs (variation: $\pm$0.5 μs). Such variation might be due to some inaccuracy in the hydrophone tilt angle to the normal direction at the curved surface. The detection stability and measurement repeatability can be improved by employing a piezoelectric detector array for conformal and stable integration on the output prism surface [42] or by using other non-contact methods (e.g., optical Doppler-interferometry probe [19]).

IV. CONCLUDING REMARKS

We demonstrated the OA prism-based multi-mode ultrasonic NDE system by simulation and experimental verification. The CNT-PDMS composite film was fabricated and utilized to realize a flexible transmitter with high OA conversion efficiency and high damage threshold. The simulation model was investigated by applying the incident angles of 33° and 61° to propagate shear and Rayleigh waves, respectively, followed by experimental confirmation with the same geometrical dimensions. The wave profiles and ToF of both wave-modes were found in good agreement with simulation results. Then, NDE application of the system allowed the detection of a circular discontinuity of 5-mm diameter by executing the incident angle of 33°, 42°, 47°, and 60° from the curved surface of input prism. The measured ToF results verified the proposed NDE system with an error less than 2% as compared to the estimated values. The high OA conversion efficiency of the CNT-PDMS transmitter enabled to detect strong acoustic signals at the detector without requiring a direct contact with the output prism, which makes the arrangement less vulnerable to damage. Our system does not require water submergence used in most of the previously reported configurations. We expect that the OA prism-based configuration for ultrasonic NDE adopting the highly efficient OA flexible transmitter can be potentially utilized for evaluation of a broad range of metallic materials. It is also capable to realize all acoustic wave-modes by incident angle variation without instigating any physical disruption or additional attenuation. Furthermore, the high damage threshold and the availability of high laser fluence enable to obtain high SNR without causing any laser ablation to transmitter or specimen.

REFERENCES

[1] S. Wang, J. Echeverry, L. Trevisi, K. Prather, L. Xiang, and Y. Liu, "Ultrahigh resolution pulsed laser-induced photoacoustic detection of multi-scale damage in CFRP composites," *Appl. Sci.*, vol. 10, no. 6, p. 2106, Mar. 2020.

[2] R. Kato, H. Endoh, and T. Hoshimiya, "Nondestructive evaluation of weld defect by photoacoustic microscopy and its destructive inspection using replica," *Jpn. J. Appl. Phys.*, vol. 50, no. 7, 2011, Art. no. 07HB04.

[3] H. Lee, H. Sohn, S. Yang, and J. Yang, "Monitoring of pipelines in nuclear power plants by measuring laser-based mechanical impedance," *Smart Mater. Struct.*, vol. 23, no. 6, Jun. 2014, Art. no. 065008.

[4] H. Liu, Y. Zhao, J. Zhou, P. Li, S.-H. Bo, and S.-L. Chen, "Photoacoustic imaging of lithium metal batteries," *ACS Appl. Energy Mater.*, vol. 3, no. 2, pp. 1260–1264, Feb. 2020.

[5] C. B. Scruby and L. E. Drain, *Laser Ultrasonics Techniques and Applications*. London, U.K.: Institute of Physics Publishing, 1990.

[6] S. Mezil, N. Chigarev, V. Tournat, and V. Gusev, "Nonlinear frequency-mixing photoacoustic characterisation of a crack," in *Measurement of Nonlinear Ultrasonic Characteristics* (Springer Series in Measurement Science and Technology). Singapore: Springer, 2020, pp. 235–281.

[7] L. Berquez, D. Marty-Dessus, and J. L. Franceschi, "Defect detection in silicon wafer by photoacoustic imaging," *Jpn. J. Appl. Phys.*, vol. 42, pp. L1198–L1200, Oct. 2003.

[8] D. Shiraishi, R. Kato, H. Endoh, and T. Hoshimiya, "Destructive inspection of weld defect and its nondestructive evaluation by photoacoustic microscopy," *Jpn. J. Appl. Phys.*, vol. 49, no. 7, 2010, Art. no. 07HB13.

[9] X. Zhang, T. Chang, Z. Wang, and H.-L. Cui, "Three-dimensional terahertz continuous wave imaging radar for nondestructive testing," *IEEE Access*, vol. 8, pp. 144259–144276, 2020.

[10] L. Yan, C. Gao, B. Zhao, X. Ma, N. Zhuang, and H. Duan, "Non-destructive imaging of standard cracks of railway by photoacoustic piezoelectric technology," *Int. J. Thermophys.*, vol. 33, nos. 10–11, pp. 2001–2005, Nov. 2012.

[11] T. Oe, Y. Nawa, N. Tsuda, and J. Yamada, "Nondestructive internal defect detection using photoacoustic and self-coupling effect," *Electron. Commun. Jpn.*, vol. 93, no. 7, pp. 17–23, Jun. 2010.

[12] D. H. Kim and U. Netzelmann, "Nondestructive testing of ceramic coatings on steel by photoacoustic, photothermal and high-frequency ultrasound techniques," *Nondestruct. Test. Eval.*, vol. 10, no. 6, pp. 343–350, Dec. 1993.

[13] K. Kim, P. Kim, J. Lee, S. Kim, S. Park, S. H. Choi, J. Hwang, J. H. Lee, H. Lee, R. E. Wijesinghe, M. Jeon, and J. Kim, "Non-destructive identification of weld-boundary and porosity formation during laser transmission welding by using optical coherence tomography," *IEEE Access*, vol. 6, pp. 76768–76775, 2018.

[14] G. Grégoire, V. Tournat, D. Mounier, and V. E. Gusev, "Nonlinear photothermal and photoacoustic processes for crack detection," *Eur. Phys. J. Special Topics*, vol. 153, no. 1, pp. 313–315, Jan. 2008.

[15] L. Liu, H. Huan, M. Zhang, X. Shao, B. Zhao, X. Cui, and L. Zhu, "Photoacoustic spectrometric evaluation of soil heavy metal contaminants," *IEEE Photon. J.*, vol. 11, no. 2, pp. 1–7, Apr. 2019.

[16] M. S. Swapna, V. P. N. Nampoori, and S. Sankararaman, "Photoacoustics: A nondestructive evaluation technique for thermal and optical characterisation of metal mirrors," *J. Opt.*, vol. 47, no. 3, pp. 405–411, Sep. 2018.

[17] S.-L. Chen, T. Ling, and L. J. Guo, "Low-noise small-size microring ultrasonic detectors for high-resolution photoacoustic imaging," *J. Biomed. Opt.*, vol. 16, no. 5, 2011, Art. no. 056001.

[18] J.-P. Monchalin and R. Heon, "Laser optical ultrasound detection using two interferometer systems," *J. Acoust. Soc. Amer.*, vol. 92, no. 1, p. 626, 1992.

[19] C. Pei, D. Yi, T. Liu, X. Kou, and Z. Chen, "Fully noncontact measurement of inner cracks in thick specimen with fiber-phased-array laser ultrasonic technique," *NDT & E Int.*, vol. 113, Jul. 2020, Art. no. 102273.

[20] P. K. Mayakuntla, D. Ghosh, and A. Ganguli, "Nondestructive evaluation of rebar corrosion in concrete structures using ultrasonics and laser-based sensing," *Nondestruct. Test. Eval.*, vol. 37, no. 3, pp. 297–314, 2022.

[21] J.-R. Lee, C. C. Chia, H. Jin Shin, C.-Y. Park, and D. J. Yoon, "Laser ultrasonic propagation imaging method in the frequency domain based on wavelet transformation," *Opt. Lasers Eng.*, vol. 49, no. 1, pp. 167–175, Jan. 2011.

[22] E. B. Flynn, J.-R. Lee, G. J. Jarmer, and G. Park, "Frequency-wavenumber processing of laser-excited guided waves for imaging structural features and defects," in *Proc. 6th Eur. Workshop Struct. Health Monit.*, Dresden, Germany, 2012, pp. 1–8.

[23] N. Hosoya, R. Umino, A. Kanda, I. Kajiwara, and A. Yoshinaga, "Lamb wave generation using nanosecond laser ablation to detect damage," *J. Vib. Control*, vol. 24, no. 24, pp. 5842–5853, Dec. 2018.

[24] S. C. Hong, J. R. Lee, S. Y. Chong, C. Y. Park, and S. Girrens, "Effect of laser pulse fatigue on the mechanical characteristic of an unpainted CFRP plate," in *Advances in Structural Health Management and Composite Structures*, vol. 12. Jeonju, South Korea: Chonbuk National Univ., 2012.

[25] E. Biagi, M. Brenci, S. Fontani, L. Masotti, and M. Pieraccini, "Photoacoustic generation: Optical fiber ultrasonic sources for non-destructive evaluation and clinical diagnosis," *Opt. Rev.*, vol. 4, no. 4, pp. 481–483, 1997.

[26] P. A. Fomitchov, A. K. Kromine, and S. Krishnaswamy, "Photoacoustic probes for nondestructive testing and biomedical applications," *Appl. Opt.*, vol. 41, no. 22, pp. 4451–4459, 2002.

[27] C. Du, J. Owusu Twumasi, Q. Tang, X. Guo, J. Zhou, T. Yu, and X. Wang, "All-optical photoacoustic sensors for steel rebar corrosion monitoring," *Sensors*, vol. 18, no. 5, p. 1353, Apr. 2018.

[28] Q.-B. Lu, T. Liu, L. Ding, M.-H. Lu, J. Zhu, and Y.-F. Chen, "Probing the spatial impulse response of ultrahigh-frequency ultrasonic transducers with photoacoustic waves," *Phys. Rev. Appl.*, vol. 14, no. 3, Sep. 2020, Art. no. 034026.

[29] W.-Y. Chang, X. A. Zhang, J. Kim, W. Huang, A. Bagal, C.-H. Chang, T. Fang, H. F. Wu, and X. Jiang, "Evaluation of photoacoustic transduction efficiency of candle soot nanocomposite transmitters," *IEEE Trans. Nanotechnol.*, vol. 17, no. 5, pp. 985–993, Sep. 2018.

[30] E. Biagi, F. Margheri, and D. Menichelli, "Efficient laser-ultrasound generation by using heavily absorbing films as targets," *IEEE Trans. Ultrason., Ferroelectr., Freq. Control*, vol. 48, no. 6, pp. 1669–1680, Nov. 2001.

[31] M. G. Joo, K.-T. Lee, P. Sang, J. Heo, H. J. Park, and H. W. Baac, "Laser-generated focused ultrasound transmitters with frequency-tuned outputs over sub-10-MHz range," *Appl. Phys. Lett.*, vol. 115, no. 15, Oct. 2019, Art. no. 154103.

[32] C. Zheng, H. Zhu, Z. Xu, R. K. Sinha, Q. Li, and P. Ghosh, "High-efficient photoacoustic generation with an ultrathin metallic multilayer broadband absorber," *Opt. Exp.*, vol. 29, no. 6, pp. 8490–8497, 2021.

[33] H. Won Baac, J. G. Ok, H. J. Park, T. Ling, S.-L. Chen, A. J. Hart, and L. J. Guo, "Carbon nanotube composite optoacoustic transmitters for strong and high frequency ultrasound generation," *Appl. Phys. Lett.*, vol. 97, no. 23, Dec. 2010, Art. no. 234104.

[34] H. W. Baac, J. G. Ok, A. Maxwell, K.-T. Lee, Y.-C. Chen, A. J. Hart, Z. Xu, E. Yoon, and L. J. Guo, "Carbon-nanotube optoacoustic lens for focused ultrasound generation and high-precision targeted therapy," *Sci. Rep.*, vol. 2, no. 1, p. 989, 2012.

[35] T. Lee, H. W. Baac, Q. Li, and L. J. Guo, "Efficient photoacoustic conversion in optical nanomaterials and composites," *Adv. Opt. Mater.*, vol. 6, no. 24, Dec. 2018, Art. no. 1800491.

[36] M. Faraz, M. A. Abbasi, P. Sang, D. Son, and H. W. Baac, "Stretchable and robust candle-soot nanoparticle-polydimethylsiloxane composite films for laser-ultrasound transmitters," *Micromachines*, vol. 11, no. 7, p. 631, Jun. 2020.

[37] Z. Sun, B. Rocha, K.-T. Wu, and N. Mrad, "A methodological review of piezoelectric based acoustic wave generation and detection techniques for structural health monitoring," *Int. J. Aerosp. Eng.*, vol. 2013, pp. 1–22, Dec. 2013.

[38] S. M. Allan, I. Baranova, J. Poley, and H. Reis, *Energy Saving Glass Lamination Via Selective Radio Frequency Heating*. Troy, NY, USA: CeraLink, 2012.

[39] V. V. Kozhushko and P. Hess, "Laser-induced focused ultrasound for nondestructive testing and evaluation," *J. Appl. Phys.*, vol. 103, no. 12, Jun. 2008, Art. no. 124902.

[40] X. Zou, N. Wu, Y. Tian, and X. Wang, "Nondestructive characterization for PDMS thin films using a miniature fiber optic photoacoustic probe," *Proc. SPIE*, vol. 8694, Apr. 2013, Art. no. 86940P.

[41] X. Zou, T. Schmitt, D. Perloff, N. Wu, T.-Y. Yu, and X. Wang, "Nondestructive corrosion detection using fiber optic photoacoustic ultrasound generator," *Measurement*, vol. 62, pp. 74–80, Feb. 2015.

[42] H. Kim, W.-Y. Chang, T. Kim, and X. Jiang, "Stress-sensing method via laser-generated ultrasound wave using candle soot nanoparticle composite," *IEEE Trans. Ultrason., Ferroelectr., Freq. Control*, vol. 67, no. 9, pp. 1867–1876, Sep. 2020.

[43] T. Lee, C. Zhang, Q. Li, L. J. Guo, and H. W. Baac, "Air-backed optoacoustic transmitter for high amplitude quasi-monopolar wave," in *Proc. IEEE Int. Ultrason. Symp.*, Sep. 2014, pp. 878–881.

[44] P. Katchadjian, C. Desimone, A. D. Garcia, D. O. Thompson, and D. E. Chimenti, "Application of axicon lenses in ultrasonic techniques," *AIP Conf. Proc.*, vol. 1211, Mar. 2010, Art. no. 1043.

MUHAMMAD AWAIS ABBASI received the B.S. degree in electronics engineering from COMSATS University Islamabad (CUI), Abbottabad Campus, Pakistan, in 2011, and the M.S. degree in electrical engineering from Government College University (GCU), Lahore, Pakistan, in 2014. He is currently pursuing the Ph.D. degree with Sungkyunkwan University, Suwon, Republic of Korea. His research interests include laser-generated ultrasound transmitters and systems for biomedical therapy and non-destructive evaluation.

HYOUNG WON BAAC (Member, IEEE) received the B.S. degree in electronic engineering from Sungkyunkwan University, Suwon, Republic of Korea, in 1999, and the Ph.D. degree in electrical engineering and computer sciences from the University of Michigan, Ann Arbor, MI, USA, in 2012. From 2012 to 2014, he was a Postdoctoral Fellow at the Wellman Center for Photomedicine, Harvard Medical School and Massachusetts General Hospital, Boston, MA, USA. He is currently an Associate Professor with the Department of Electrical and Computer Engineering, Sungkyunkwan University. His current research interests include laser-generated ultrasound systems and optical/acoustic sensors for biomedical therapy, healthcare, and non-destructive evaluation.